

Unravelling the Effects of Layered Supports on Ru Nanoparticles for Enhancing N₂ Reduction in Photocatalytic Ammonia Synthesis

Huimin Liu ^{[a,b], 1}, Ping Wu ^{[b], 1}, Haitao Li ^[a], Zibin Chen ^[c], Lizhuo Wang ^[a], Xin Zeng ^[a], Yuxiang Zhu ^[d], Yijiao Jiang ^[d], Xiaozhou Liao ^[c], Brian S. Haynes ^[a], Jinhua Ye ^{[c]*}, Catherine Stampfl ^{[b]*}, Jun Huang ^{[a]*}

[a] Laboratory for Catalysis Engineering, School of Chemical and Biomolecular Engineering, The University of Sydney, Chemical Engineering Building J01, Sydney, New South Wales 2006, Australia.
E-mail: Jun.huang@sydney.edu.au

[b] School of Physics, The University of Sydney, Sydney, New South Wales 2006, Australia
E-mail: Catherine.stampfl@sydney.edu.au

[c] School of Aerospace, Mechanical and Mechatronic Engineering, The University of Sydney, Sydney, NSW 2006, Australia

[d] Department of Engineering, Macquarie University, Sydney, New South Wales 2109, Australia

[e] International Center for Materials Nanoarchitectonics (WPI-MANA), National Institute for Materials Science (NIMS), 1-1 Namiki, Tsukuba, Ibaraki 305-0044, Japan

ABSTRACT:

Harnessing the vast supply of solar energy as the driving force to produce ammonia from abundant nitrogen gas and water is beneficial for both relieving energy demands and developing sustainable chemical industry. Bulk carbon nitride (B-g-C₃N₄), exfoliated carbon nitride (E-g-C₃N₄) and graphite (g-C) supported Ru-K catalysts, denoted as Ru-K/B-g-C₃N₄, Ru-K/E-g-C₃N₄ and Ru-K/g-C, respectively, with the layered materials serving both as supports and light harvesters, were designed for photocatalytic ammonia synthesis. It was discovered that, besides the light harvesting properties of the catalysts which played roles in photocatalytic reactions, the structure of the supports influenced greatly the preferential locations of Ru species, which further exerted effects on the N₂ activation process and ultimately impacted the ammonia production rate. The fine Ru nanoparticles uniformly and randomly dispersed on the monolayered E-g-C₃N₄ did not provide outstanding activity in ammonia photosynthesis; in contrast, Ru nanoparticles at the step edges of bulk g-C₃N₄ exhibited lower overall barriers for N₂ activation and a much enhanced photocatalytic ammonia synthesis rate due to the synergy effects between metal and support as confirmed by density functional theory (DFT) calculations. The discovery of the relationship between reactivity and support geometry in this study will be important in guiding the rational predesign of efficient photocatalysts.

KEYWORDS: Ammonia synthesis; layered support; Ru-based catalysts; Synergy effects between metal and support; N₂ activation

Introduction

Owing to its use in the fertilizer industry and in creating building blocks for the synthesis of various pharmaceutical products, ammonia (NH_3) is recognized as one of the mainstays in the modern world, with 160 million tons of ammonia being synthesized per year ^[1-4]. However, the industrialized Haber-Bosch process suffers from a number of disadvantages, such as using high value-added clean energy H_2 and requiring harsh reaction conditions (temperatures: 400-500 °C and pressures: >60 bar) ^[5-6]. In this respect, it will be of great significance to develop a low-cost approach for ammonia synthesis, which could be carried out under mild reaction conditions.

Photocatalytic reduction of nitrogen with water is a promising alternative route for ammonia synthesis. On one hand, water, the cheapest and most abundant hydrogenated resource, has proven to be a favourable substitute for H_2 in ammonia synthesis in several pioneering studies ^[7-8]; and on the other hand, photoreduction of nitrogen to ammonia using solar light is a sustainable and green ammonia synthesis route ^[9-11]. Several semiconductors, including bismuth oxyhalides, titanium dioxide and ultrafine $\text{Bi}_5\text{O}_7\text{Br}$, have been used for photocatalytic ammonia production ^[7-11]. Nevertheless, the efficiencies of these photocatalysts are still low. Therefore, it remains of great importance to develop a photocatalyst which could drive the nitrogen reduction process efficiently.

For the photocatalytic ammonia synthesis process, the cleavage of strongly bonded $\text{N}\equiv\text{N}$ bond (945 kJ mol^{-1}) is the rate determining step ^[12-14]. Previous research has revealed that high photocatalytic nitrogen reduction activities and ammonia synthesis capacities could be achieved by introducing transition metals, such as Fe or Ru, to semiconductors for promoting the $\text{N}\equiv\text{N}$ cleavage process ^[15-21]. In comparison to Fe, Ru is more favourable for $\text{N}\equiv\text{N}$ activation because it requires relatively mild reaction conditions ^[15-16] and high catalytic activities can be achieved by adding alkali or alkaline earth metals, such as K or Ba, as promoters.

It has been widely reported that the architecture and interaction between supports and metal nanoparticles could significantly influence the activities of metal nanoparticles in the catalytic reactions ^[22-25]. For photocatalytic ammonia synthesis via N_2 fixation, although several studies have been carried out over Ru/semiconductor catalysts ^[26-29], to the best of our knowledge, there have been no reports on investigating the structural effects of the semiconductor support on the photocatalytic performance. Therefore, it is important to investigate this unexplored area, since its success will definitely contribute new knowledge and foster the development of the targeted research area.

Two dimensional semiconductors have been widely used as supports of photocatalysts in the form of either their bulk particles or exfoliated monolayers, with monolayered supports generally being considered to contribute higher activities than their bulk counterparts [30-32]. Among the numerous two dimensional semiconductors, graphitic carbon nitride (g-C₃N₄) is attracting significant attention and has been extensively investigated in the area of photocatalysis because of its remarkable light harvesting capacity in the visible light region [33-35]. Further, g-C₃N₄, including both bulk g-C₃N₄ (B-g-C₃N₄) and exfoliated g-C₃N₄ (E-g-C₃N₄), has proven to be capable of activating nitrogen with light irradiation [36-39]. In the present study, both bulk and exfoliated forms were adopted as supports for Ru-based catalysts for photocatalytic ammonia production. In addition, commercial graphite (g-C), a material with a layered structure similar to that of B-g-C₃N₄ but with a very different response to light irradiation, was employed as a reference support. The physicochemical and photoelectrical properties of the supports and catalysts were characterized in detail to establish the relationship between reactivity and support/catalyst geometry with the assistance of theoretical simulations, which will be important in guiding the rational predesign of efficient photocatalysts for ammonia synthesis.

Experiment

Catalyst preparation

Urea, iso-propanol, KNO₃, RuCl₃ and g-C were commercial from Sigma-Aldrich and used as received. Bulk carbon nitride (B-g-C₃N₄) was prepared by thermally decomposing urea at 550 °C for 4 h [40]. E-g-C₃N₄ was synthesized by exfoliating B-g-C₃N₄ by the ultrasonic method [41]. Typically, 100 mg B-g-C₃N₄ was dispersed in 100 mL iso-propanol, and sonicated for 10 h. The suspension was subsequently centrifuged at 5000 rpm and 22000 rpm, respectively, to remove the un-exfoliated B-g-C₃N₄. The precipitate was then dried at 80 °C to obtain E-g-C₃N₄.

Catalysts Ru-K/B-g-C₃N₄, Ru-K/E-g-C₃N₄ and Ru-K/g-C were prepared via incipient wetness impregnation method in consecutive steps, firstly with KNO₃ followed by RuCl₃ solution. In the study, the theoretical loadings of K and Ru were controlled as 5.0 wt% and 2.0 wt%, respectively. Before characterization and reaction evaluation, the catalysts were calcined in 5% H₂/Ar at 400 °C for 4 h to remove Cl residue and reduce Ru to the metallic state.

Catalyst characterization

The crystalline structures of the catalysts were analysed by an X-ray diffractometer (XRD, SIEMENS D5000) using Cu K α radiation (wavelength of 0.1542 nm). The surface area, average pore size, and total pore volume of the samples were determined by measuring the N₂ adsorption-desorption isotherms on an Autosorb IQ-C system. The light absorption properties of the catalysts were carried out over a UV-visible

spectroscopy (Shimadzu, UV-3800 Plus). The morphology of the supports and catalysts were characterized by transmission electron microscopy (TEM, JEOL 3000). The actual contents of Ru and K over the catalysts, as well as the leaching of Ru and K over the catalysts during reaction evaluation, were analysed by inductively coupled plasma atomic emission spectroscopy (ICP-AES, Varian 720-ES). The photocurrents of the supports and catalysts were measured on a CHI electrochemical analyser using a standard three-electrode mode with 0.5 M Na₂SO₄ solution as the electrolyte.

Catalyst evaluation

The catalytic performance for the ammonia synthesis reaction was carried out in a 100 mL Teflon-lined, quartz-windowed autoclave. 3.0 mg of the catalyst was dispersed into 15.0 mL deionized water, with 1.0 mL methanol serving as the sacrificial agent. The autoclave was exchanged by 2.0 bar N₂ ten times to remove inside residual air and then refilled by 2.0 bar N₂. The reaction was maintained for several hours with stirring and light irradiation (PE300 Xe lamp). The amount of ammonia production was identified by the indophenol blue method. As reference, the catalytic performance of Ru-K/B-g-C₃N₄ and Ru-K/E-g-C₃N₄ for the hydrogen evolution reaction were also carried out, with the procedure the same as the one for the ammonia synthesis process, except that Ar, instead of N₂, was used.

Theoretical calculations

Spin-polarized density functional theory (DFT) calculations were performed using the VASP software.^[42-43] The generalized gradient approximation of Perdew, Burke and Ernzerhof (PBE)^[44] was used for the exchange-correlation functional. The kinetic energy cut-offs were well tested to yield good convergence of the total energy, where 500 eV was used for all calculations. To correctly describe the strong van der Waals interactions between the neighboring g-C₃N₄ layers, the DFT-D₃ approach of Grimme was applied.^[45] A Monkhorst-Pack grid was used and the mesh of k-points (3×3×1 for E-g-C₃N₄ and 1×3×1 for B-g-C₃N₄) was well tested for the structure relaxation and the total energy calculations. The climbing image nudged elastic band (CINEB) method was used for transition-state searches and barrier height determination.^[46] Residual forces were within 0.02 eV/Å for geometry optimizations and 0.03 eV/Å for transition-state location.

The calculated lattice constants of bulk g-C₃N₄ are a=b=7.13 Å and c=3.245 Å, in good agreement with the previous theoretical calculations (a=b=7.178 Å, c=3.297 Å^[47] and a=b=7.11 Å, c=3.19 Å^[48]). The adsorption energy was defined as $E_{\text{abs}} = E_{\text{total}} - E_{\text{species}} - E_{\text{sub}}$, where E_{total} , E_{sub} and E_{species} are the total energy of the whole system, the clean support surface, and reaction gas or metal cluster in vacuum, respectively.

Calculation of the size of [Ru(H₂O)₆]³⁺

The precursors in solution exist as $[\text{Ru}(\text{H}_2\text{O})_6]^{3+}$. $[\text{Ru}(\text{H}_2\text{O})_6]^{3+}$ is octahedral, with a Ru-O bond length of 0.214 nm^[49], so the diameter size of $[\text{Ru}(\text{H}_2\text{O})_6]^{3+}$ would be at least 0.42 nm (0.428nm=2×0.214 nm).

Results and discussion

The XRD pattern of commercial g-C revealed the representative diffraction peak for carbon based materials at 27.3 ° (Figure 1a)^[51]. As-prepared B-g-C₃N₄ and E-g-C₃N₄ exhibited the typical diffraction feature of g-C₃N₄ at 13.9 ° and 27.8 ° (Figure 1a), with the two peaks resulting from the graphite structure and tri-s-triazine units, respectively^[33-39]. The successful exfoliation of E-g-C₃N₄ was confirmed by comparing its properties with its precursor B-g-C₃N₄. As shown in Table 1 and Figure S1, the surface area is increased from 35.3 to 88.0 m² g⁻¹. The light absorption edge of E-g-C₃N₄ locates at a shorter wavelength (Figure 1b and Figure S2). Figure 2a shows E-g-C₃N₄ has a wider optical bandgap than B-g-C₃N₄. A slightly shifted peak in the photoluminescence spectrum was found in E-g-C₃N₄ (Figure S3). The photocurrent of E-g-C₃N₄ in Figure 2b is also enhanced due to its good electron-hole separation and transport properties. The TEM image of E-g-C₃N₄ is much more transparent (Figure 3a) than those of g-C (Figure 3b) and B-g-C₃N₄ (Figure 3c)^[33-39].

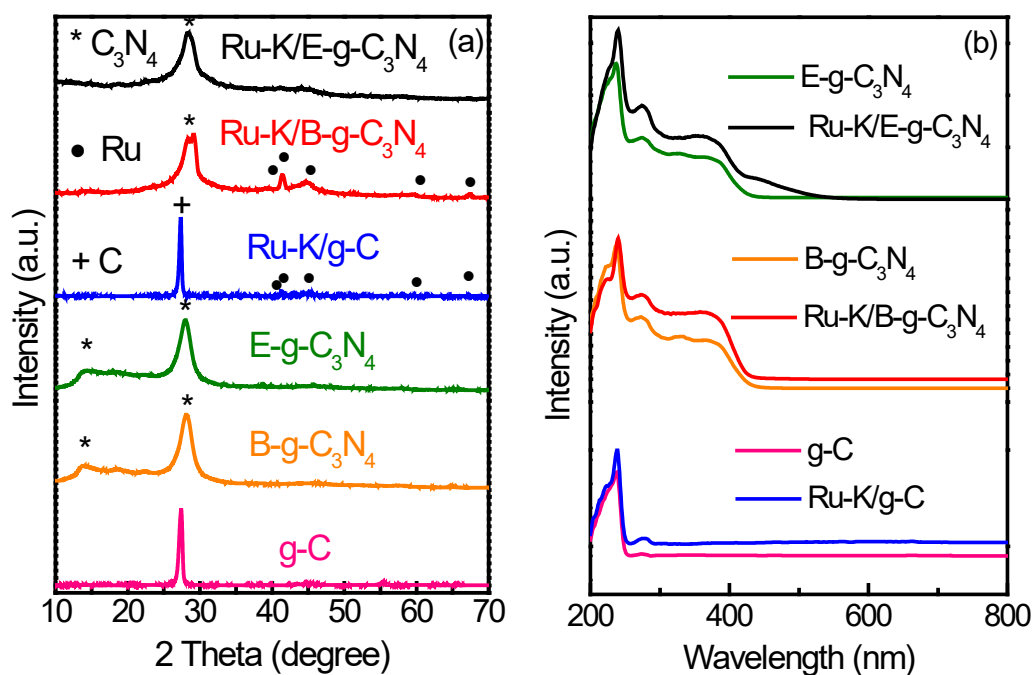


Figure 1 (a) XRD diffraction patterns (the symbols *, • and + represent C₃N₄, Ru and C, respectively), and (b) UV-visible spectra of supports and catalysts.

Table 1 Physicochemical properties of the supports and catalysts.

Support/Catalyst	S_{BET} ($\text{m}^2 \text{g}^{-1}$) ^a	Ru content (wt. %) ^b	K content (wt. %) ^b
graphite	16.2	-	-
B-g-C ₃ N ₄	35.3	-	-
E-g-C ₃ N ₄	88.0	-	-
Ru-K/graphite	3.8	1.76	4.30
Ru-K/B-g-C ₃ N ₄	24.5	1.80	4.09
Ru-K/E-g-C ₃ N ₄	52.5	1.67	3.76

^a obtained by the N₂ adsorption-desorption method through the Brunauer-Emmett-Teller equation.

^b analyzed by ICP-AES method.

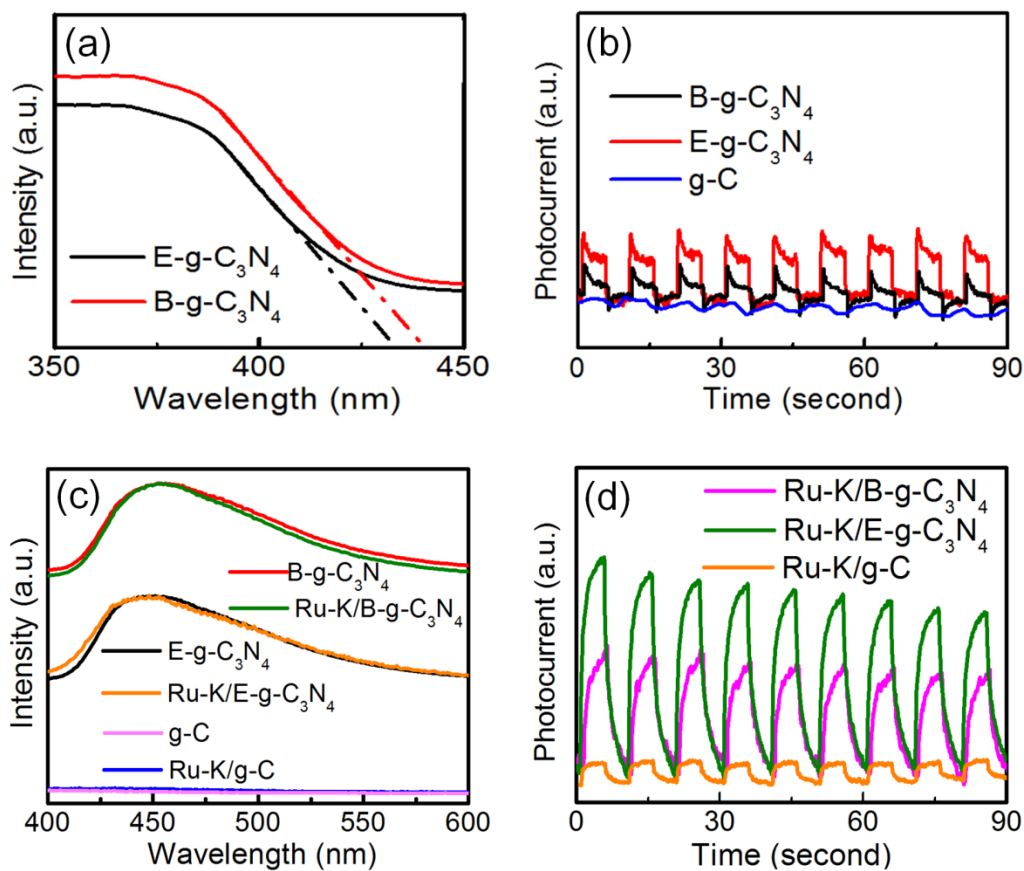


Figure 2 (a) Enlarged UV-visible spectra of B-g-C₃N₄ and E-g-C₃N₄ in the range of 350-450 nm. (b) Photocurrents over the supports. (c) Photoluminescence spectra and (d) photocurrents of supports and catalysts.

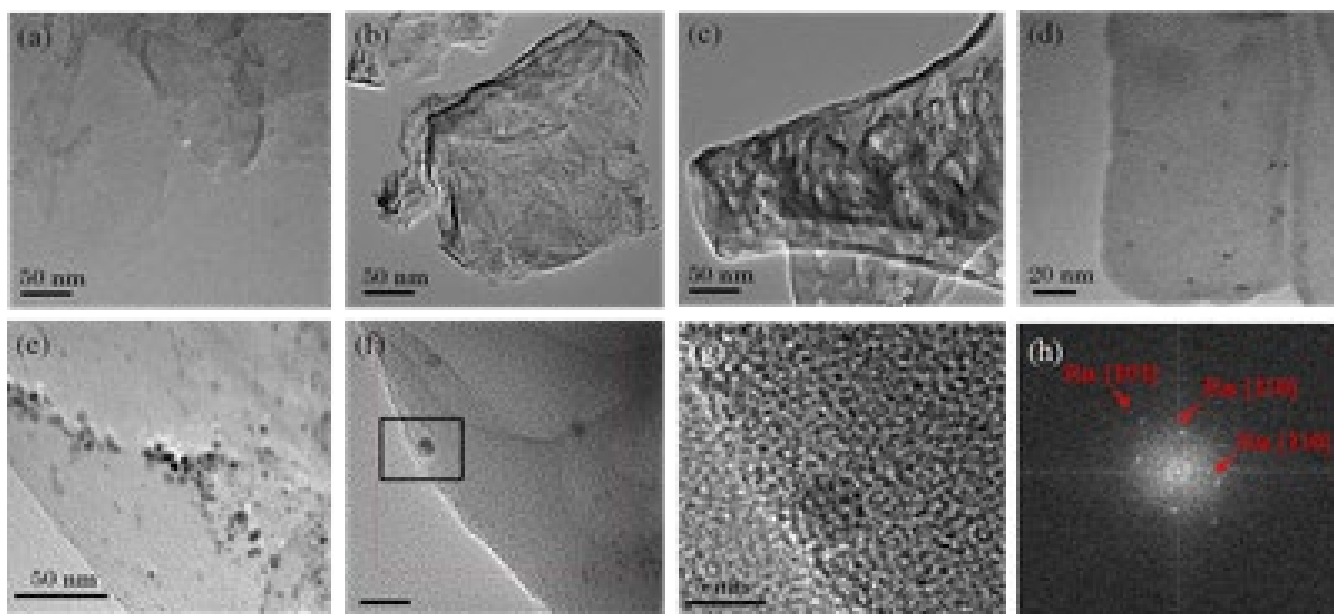


Figure 3 TEM images of the supports and catalysts. (a) E-g-C₃N₄, (b) g-C, (c) B-g-C₃N₄, (d) Ru-K/E-g-C₃N₄, (e) Ru-K/g-C, (f) Ru-K/B-g-C₃N₄, (g) high resolution TEM image of Ru-K/B-g-C₃N₄ in Figure 2f, and (h) FFT image of the particle in Figure 2g.

After the loading of Ru and K, obvious diffraction peaks attributed to metallic Ru were observed over Ru-K/g-C and Ru-K/B-g-C₃N₄, which are attributed to the unfavourable dispersion of Ru species on the supports with smaller specific surface areas (Figure 1a, Table 1 and Figure S1). Over Ru-K/E-g-C₃N₄, no diffraction peaks assigned to metallic Ru were detected (Figure 1a), suggesting that the Ru nanoparticles were very fine and well dispersed over E-g-C₃N₄. Even though the loadings of K were high (up to ca. 4 wt. %, Table 1), no diffraction peaks attributable to K species were observed in any of the catalysts, indicating that K species were of very small structures, highly dispersed over the three supports (Figure 1a). The shift of representative diffraction peak for g-C₃N₄ to high values is probably due to the lattice distortion resulted by the doped Ru and K. The dispersion behaviours of Ru particles and K species over the Ru-K catalysts were further confirmed via their TEM images in Figure 3d-3h. As in this study, two metals were loaded onto a specific support, it is important to distinguish the two metals from each other. Here, the crystalline structure and the fast fourier transform (FFT) diffraction spot analysis of all the observable nanoparticles were carried out to identify their compositions, with the nanoparticles displaying in the square of the TEM image of Ru-K/B-g-C₃N₄ in Figure 3f as a typical example. Its high resolution TEM image (Figure 3g), together with the FFT diffraction spots at 2.05 Å and 1.35 Å (Figure 3h) which

could be assigned to the (101) and (110) planes of hexagonal close-packed Ru^[51], suggest that the nanoparticle was metallic Ru. All the observable nanoparticles were confirmed to be metallic Ru while K species were not detected, indicating K was well dispersed with very small sizes. The average sizes of Ru nanoparticles over Ru-K/E-g-C₃N₄, Ru-K/g-C and Ru-K/B-g-C₃N₄ could be obtained from the TEM images in Figures 3d-3f, and they were 2.8 nm, 6.9 nm and 4.2 nm, respectively. The light absorption properties (Figure 1b), photoluminescence properties (Figure 2(c)) and the trend in photocurrents (Figure 2(d)) were not influenced greatly after the loading of Ru and K. The trend in photocurrents is Ru-K/E-g-C₃N₄ > Ru-K/B-g-C₃N₄ > Ru-K/g-C.

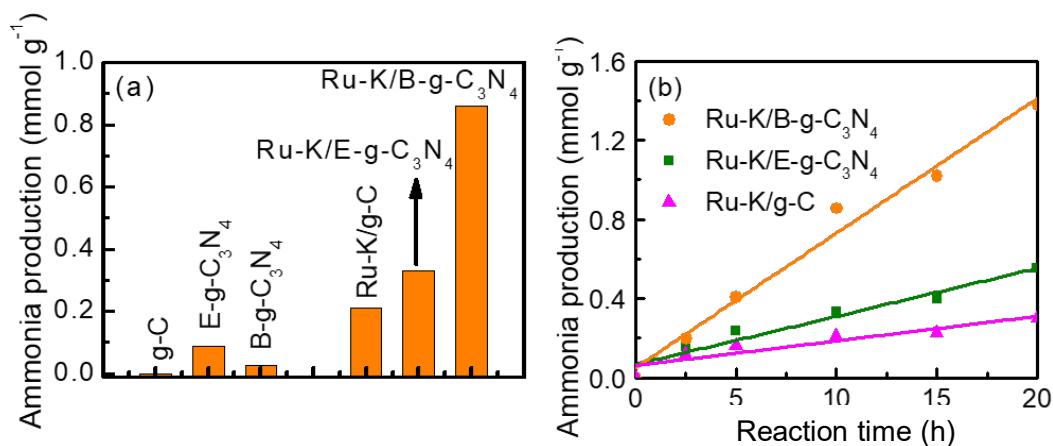


Figure 4 (a) The amount of ammonia production over the supports and catalysts with a reaction time of 10 hours, and (b) effects of reaction time on the amount of ammonia production over Ru-K/B-g-C₃N₄, Ru-K/E-g-C₃N₄ and Ru-K/g-C.

The detailed results for photocatalytic ammonia synthesis are displayed in Figure 4. As expected, g-C exhibited nearly no catalytic activity because of its poor light absorption capacity (Figure 1b), while B-g-C₃N₄ and E-g-C₃N₄ exhibited some but low activities for ammonia production (0.00-0.08 mmol g⁻¹ ammonia production at 10 hours reaction), with the activities over the supports conforming to the trend of E-g-C₃N₄ > B-g-C₃N₄ > g-C (Figure 4a). The higher activity over E-g-C₃N₄ relative to that over B-g-C₃N₄ is due to its larger specific surface area, and more efficient electron/hole separation and transport processes (Table 1 and Figure 2b) [33-39].

Introducing Ru and K in order to promote N₂ activation increased ammonia production from 0.00-0.08 mmol g⁻¹ up to 0.21-0.85 mmol g⁻¹ after 10 hours reaction (Figure 4a). We had expected E-g-C₃N₄, combined with the highly dispersed and fine Ru particles on Ru-K/E-g-C₃N₄, to be more active in ammonia synthesis compared to the Ru particles poorly dispersed on B-g-C₃N₄ with lower surface area (Ru-K/B-g-C₃N₄), however, the yield of ammonia production over Ru-K/B-g-C₃N₄ (0.85 mmol g⁻¹) was nearly 2.6 times higher than that over Ru-K/E-g-C₃N₄ (0.33 mmol g⁻¹) after 10 hours reaction, opposite to the above

expectation. The activity tests, as the function of time in Figure 4b, further confirmed the trend of ammonia production rates as Ru-K/B-g-C₃N₄ > Ru-K/E-g-C₃N₄ > Ru-K/g-C. ICP-AES analysis of the post-reaction aqueous solutions revealed that the leaching of Ru and K over the catalysts could be neglected during 10 h evaluation (Table S2).

It is considered whether the NH₂/NH groups on g-C₃N₄ would be consumed during the reaction and contribute to ammonia synthesis. It can be stated that the NH₂/NH groups on g-C₃N₄ has negligible contribution to the overall ammonia production due to the following three reasons. (1) Over each of the catalysts, the amount of ammonia production increased nearly linearly with reaction time (Figure 4b), indicating that the ammonia synthesis was not based on the consumption of NH₂/NH groups. The reason is that, if the NH₂/NH group contributed significantly to ammonia production, more ammonia would be generated at the initial stage of the reaction, and the reaction rate decreased gradually with the consumption of NH/NH₂ groups. (2) The *sp*³ C-N bond is quite stable and the dissociation energy is about 3.39 eV^[52], while the adsorption energy of NH/NH₂ on Ru surface is 1.02/1.72 eV^[53]. Thus, the cleavage of C-N bond and formation of Ru-N bond should need high energy to overcome the energy barrier. (3) Given the same molecular formula between E-g-C₃N₄ and B-g-C₃N₄, E-g-C₃N₄ should possess the same amounts of NH₂/NH as B-g-C₃N₄ if the same amounts of g-C₃N₄ were used as photocatalyst, which then leads to comparable or higher photocatalytic performance over E-g-C₃N₄ than B-g-C₃N₄ (by taking the facilitated electron-hole separation over E-g-C₃N₄ into consideration). However, the ammonia yield on B-g-C₃N₄ was higher than E-g-C₃N₄.

Considering that photocatalytic ammonia production is a tandem reaction, comprising two consecutive reactions, photocatalytic H₂ evolution and ammonia synthesis from N₂ and H₂, respectively, photocatalytic H₂ evolution activities over Ru-K/E-g-C₃N₄ and Ru-K/B-g-C₃N₄ were evaluated for reference. It was found that, over a 10 h reaction period, H₂ production amounted to 2.1 mmol g⁻¹ and 2.9 mmol g⁻¹ over Ru-K/B-g-C₃N₄ and Ru-K/E-g-C₃N₄, respectively. Furthermore, H₂ generation could also be detected over Ru-K/B-g-C₃N₄ and Ru-K/E-g-C₃N₄ catalysts during the ammonia synthesis process. This suggests that H₂ or H radical generation is not the rate-determining step in the ammonia synthesis and that Ru-K/E-g-C₃N₄ exhibits greater activity than Ru-K/B-g-C₃N₄ in photocatalytic reactions, consistent with the greater electron-hole separation capacity of E-g-C₃N₄^[33-39]. We therefore conclude that the second reaction, ammonia synthesis from N₂ and H₂, is the rate-determining step, and that the synergetic effects between Ru and g-C₃N₄ other than photo-properties, must be responsible for the significant enhancement of the N₂ dissociation and reaction with H₂ that lead to the greater ammonia production rate over Ru-K/B-g-C₃N₄.

The TEM image of Ru-K/B-g-C₃N₄ revealed that the Ru particles preferred to stay on the edges of the support B-g-C₃N₄ (Figure 3f), and a similar phenomenon was also observed for the Ru particles on Ru-

K/g-C (Figure 3e). In contrast, the TEM image of Ru-K/E-g-C₃N₄ in Figure 3d revealed that the Ru particles were relatively uniformly dispersed on E-g-C₃N₄, and no obvious location preference was observed. As the TEM images (Figure 3a-3c) revealed, E-g-C₃N₄ was monolayer/few-layer structured, while B-g-C₃N₄ and g-C were multilayered. This raised the questions of whether the layered structure of the supports could exert an influence on the locations of Ru particles and K species, which we investigate below.

As described in the catalyst preparation section, Ru and K are loaded onto the catalyst by exposure to aqueous solutions of their salts. We note that the precursors in solution exist as Ru(H₂O)₆³⁺ [54] and K⁺, which have cation diameters of 0.42 nm and 0.14 nm [55], respectively. Compared to the layer spacing of ca. 0.32 nm [33-39] in B-g-C₃N₄ and g-C, it is apparent that the observed high degree of dispersion of K is consistent with its being able to move easily into the interlayer region which is not accessible to the larger Ru precursor in these substrates. Instead, over B-g-C₃N₄ and g-C, Ru is concentrated at the step edges between layers presumably because these low-coordinated, high specific surface-energy sites promote Ru nucleation. The more uniform dispersion of Ru over the exfoliated E-g-C₃N₄ is consistent with the limited interlayer space and scant numbers of steps on E-g-C₃N₄. The H₂-TPR profiles of Ru-K/E-g-C₃N₄ in Figure S4 showed no peak for Ru reduction probably because the Ru NPs is too small and the reduction process was proceeded gradually; while an obvious peak for Ru reduction at around 240~250 °C was found in the Ru-K/B-g-C₃N₄, which suggested the interaction between Ru and carbon support is stronger on the Ru-K/B-g-C₃N₄ than the Ru-K/E-g-C₃N₄ due to the edge effect.

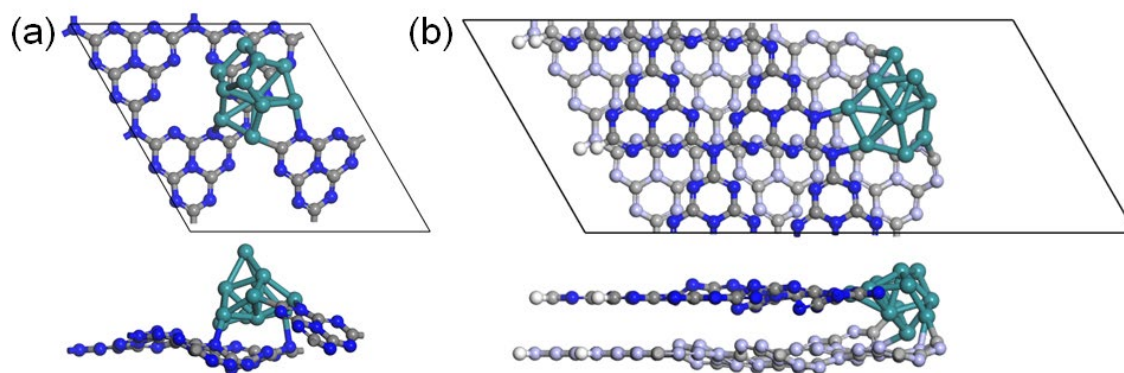


Figure 5. Top and side views of the most stable geometric structures of Ru₁₁ cluster adsorption on (a) E-g-C₃N₄ and (b) B-g-C₃N₄ supports. The gray, blue and cyan balls represent C, N and Ru atoms, respectively. In the second layer of B-g-C₃N₄, the light gray and light blue atoms represent C and N, respectively. We conclude that the unexpected significant enhancement of ammonia production over Ru-K/B-g-C₃N₄ is due to the location of the Ru at the edge steps where apparently poor dispersion nevertheless gives greater activity than the well-dispersed Ru in Ru-K/E-g-C₃N₄. Therefore, DFT calculations were carried out to confirm and explore the underlying reaction mechanisms. To model the Ru-K/E-g-C₃N₄ catalyst, a

Ru₁₁ cluster was adsorbed on an E-g-C₃N₄ layer where various adsorption sites were considered, and for the Ru-K/B-g-C₃N₄ catalyst, the Ru₁₁ cluster was placed at the edge of two layers of g-C₃N₄ (the illustrations of the supports are displayed in Figure S5). Here, the Ru₁₁ cluster was chosen because it is the smallest cluster containing sites like the B₅ step sites^[3, 16], which are viewed as the active centers for N₂ dissociation (the atomic structure of Ru₁₁ and the B₅ step sites are shown in Figure S6-S7). The presence of K was not considered in the simulations for the following three reasons, (1) K was well dispersed over the catalysts, (2) its function as an electron donor for Ru species has been well studied previously^[55-57], (3) roughly, the ratio of Ru species to its adjacent K species over Ru-K/E-g-C₃N₄ was 0.5 (Table 1 and Figure 2), which was a more favourable ratio for ammonia synthesis than that for Ru-K/B-g-C₃N₄ (much larger than 0.5, Table 1 and Figure 2) according to previous studies^[56-58], and (4) the introduced K atom does significantly affect the dissociation energy of N₂ (detailed simulation procedures are available in supporting information, Figure S8-S11).

As shown in Figure 5, it is found that for Ru₁₁ on E-g-C₃N₄, the Ru₁₁ cluster preferred to adsorb on the junction site where three tri-s-triazine units are linked, with an adsorption energy of -10.21 eV; while on B-g-C₃N₄, the most stable site for the Ru₁₁ cluster was on the top of the tri-s-triazine unit, where the adsorption energy was calculated to be -13.77 eV. After the introduction of the Ru₁₁ cluster, the distortion of g-C₃N₄ in the Ru/B-g-C₃N₄ catalyst was found to be greater than that in the Ru/E-g-C₃N₄ catalyst, which suggested the *sp*²-hybridization of nitrogen and carbon atoms near the edge of B-g-C₃N₄ was changed into *sp*³-hybridization, resulting in a much stronger binding between the Ru₁₁ cluster and the B-g-C₃N₄ support. The stronger binding between the Ru₁₁ cluster and B-g-C₃N₄ support is due to the electronic effects of edge sites^[59-62], since Ru₁₁ preferentially binds at the edges of B-g-C₃N₄.

In the photocatalytic ammonia synthesis reaction, the Ru₁₁ cluster can not only enhance the generation of charge carriers upon light adsorption but also provides an active centre for the proton reduction and ammonia synthesis. The ability of the Ru cluster to trap electrons is determined by the work function of the Ru^[63-64]. In our systems, considering the work function of bulk Ru of 5.4 eV^[65], the work function of Ru₁₁ cluster should be larger than those of E-g-C₃N₄ (4.13 eV) and two-layered g-C₃N₄ (3.93 eV)^[66] (Figure S13-S14), which indicates electrons flow from E-g-C₃N₄ and B-g-C₃N₄ into the Ru clusters on contact. The negatively charged Ru₁₁ cluster on the g-C₃N₄ support not only can greatly promote the photocatalytic activities of E-g-C₃N₄ and B-g-C₃N₄, in agreement with our experimental results (Figure 1b), but also mimic the function of the MoFe-cofactor in nitrogenase for N₂ reduction to NH₃.^[67-68] In the following we consider two reaction paths of ammonia synthesis, including the direct N₂ dissociation and associative N₂ dissociation mechanisms^[69]. As shown in Figure 6a, for the system of Ru/E-g-C₃N₄, ini-

tially N_2 favoured adsorption on the Ru atom of the Ru_{11} cluster perpendicularly, with an adsorption energy of -2.18 eV. Along the favourable reaction path, N_2 assumed a more parallel orientation to the surface with both N atoms bonding to the Ru_{11} cluster. This “lying-down” configuration was less stable (by 0.83 eV than the perpendicular geometry). The energy barrier from the “perpendicular” to “lying-down” orientation was calculated to be 1.13 eV. Subsequently, N_2 may undertake two different activation pathways: (1) direct N_2 dissociation, in which N_2 directly dissociates into two N atoms with the energy barrier of 1.00 eV; or alternatively (2) associative N_2 dissociation, in which the “lying-down” N_2 molecule was firstly hydrogenated to form $*N_2H$ and then dissociated into $*N$ and $*NH$, with energy barriers of 0.81 eV and 0.41 eV respectively. Therefore, over $Ru/E-g-C_3N_4$, the rate-limiting step is the change in N_2 orientated from the “perpendicular” to “lying-down” state, with the energy barrier for N_2 activation of 1.13 eV, and the associative reaction mechanism significantly more favourable than the direct N_2 dissociation mechanism.

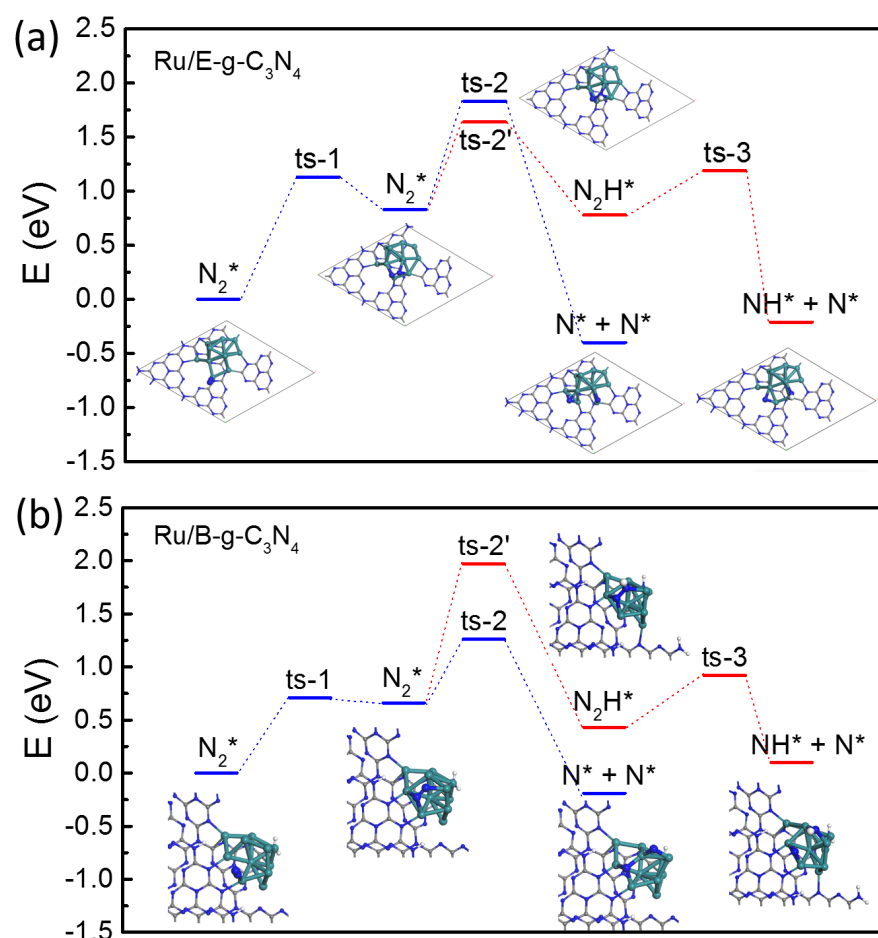


Figure 6 Direct N_2 dissociation and associative N_2 dissociation reaction mechanisms over (a) $Ru/E-g-C_3N_4$ and (b) $Ru/B-g-C_3N_4$. The reference energy (the total energy of the initial N_2 adsorption state over both supports) is set zero.

Figure 6b illustrates the two N₂ dissociation paths (direct and associative) over Ru/B-g-C₃N₄. Similarly, N₂ initially adsorbed on the Ru₁₁ cluster in a perpendicular orientation with an adsorption energy of -1.31 eV, which was lower than that on the Ru/E-g-C₃N₄ catalyst. Then, N₂ tilted and changed to a “lying-down” configuration, with an energy barrier of 0.71 eV. Following, (1) the “lying-down” N₂ can be directly dissociated with an energy barrier of just 0.60 eV, much lower than that over Ru/E-g-C₃N₄; or (2), for the associative dissociation path, the energy barriers of N₂ hydrogenation to *N₂H and dissociation of *N₂H into *N and *NH were 1.31 eV and 0.49 eV, respectively. Therefore, the direct N₂ dissociation path was much more favourable over the Ru/B-g-C₃N₄ catalyst. The tilting process of N₂ over Ru/B-g-C₃N₄ is the rate-limiting step, and the energy barrier was 0.71 eV.

The DFT results revealed that the two catalysts exhibited different underlying mechanisms for N₂ activation, namely an associative dissociation path over Ru/E-g-C₃N₄, and a direct dissociation path over Ru/B-g-C₃N₄. They, however, exhibited the same rate determining step, that is, the transition of N₂ from a perpendicular geometry to “lying down” geometry, where the energy barrier of the transition state over Ru/E-g-C₃N₄ (1.13 eV) was 0.42 eV higher than that over Ru/B-g-C₃N₄ (0.71 eV). The energy barriers 1.13 eV and 0.71 eV could be easily satisfied by light irradiation, which is why ammonia could be produced over the catalysts with light irradiation. The relative low energy barrier of the rate-limiting step over Ru/B-g-C₃N₄ suggested that the reaction rate of ammonia production over Ru/B-g-C₃N₄ will be superior to Ru/E-g-C₃N₄, in accordance with our experimental results of catalytic activity for ammonia synthesis. The lower energy barrier over Ru/B-g-C₃N₄ is attributed to the stronger binding between the Ru₁₁ cluster and the support, which reduces the interaction between N₂ and Ru₁₁ cluster.

Conclusion

In summary, the physicochemical properties of the catalysts and the evaluation results revealed that, in contrast to our general understanding that the catalyst with faster electron/hole separation rate and higher photocurrent as well as fine and well dispersed metal nanoparticles (Ru-K/E-g-C₃N₄) should exhibit better photocatalytic activity, Ru-K/B-g-C₃N₄ yielded higher photocatalytic ammonia production rate than Ru-K/E-g-C₃N₄. It is suggested that the light harvesting properties of the catalysts must cooperate with the surface reaction properties to facilitate the ammonia synthesis process. Ru nanoparticles at the edge steps over the multilayered bulk support (B-g-C₃N₄) contributed higher surface reactivity than the Ru nanoparticles uniformly and randomly dispersed over monolayered E-g-C₃N₄ in N₂ reduction with H₂. Our theoretical studies revealed that the Ru nanoparticles located at the edges possessed stronger binding with the support and exhibited a lower reaction barrier for N₂ activation, which is ultimately responsible for the

much-enhanced photocatalytic ammonia synthesis rate over Ru-K/B-g-C₃N₄. In this study, the relationship between photocatalytic reactivity and support geometry was discovered, which will be important in guiding the rational redesign of efficient photocatalysts.

APPENDIX A. SUPPLEMENTARY DATA

Figure S1-S14 about the catalyst characterization, evaluation and theoretical calculation details are shown in supporting information. This material is available free of charge via the Internet at doi:<https://doi.org/>

AUTHOR INFORMATION

Corresponding Author

* Jinhua Ye, email: Jinhua.Ye@nims.go.jp

* Catherine Stampfl, email: Catherine.stampfl@sydney.edu.au

* Jun Huang, email: Jun.huang@sydney.edu.au

Author Contributions

¹ These authors contributed equally to this work. The manuscript was written through contributions of all authors. All authors have given approval to the final version of the manuscript.

ACKNOWLEDGMENT

J.H. and C.S. acknowledge the financial supports from Australian Research Council Discovery Projects (DP150103842).

REFERENCES

- [1] Kitano, M.; Inoue, Y.; Yamazaki, Y.; Hayashi, F.; Kanbara, S.; Matsuishi, S.; Yokoyama, T.; Kim, S.; Hara, M.; Hosono, H. *Nat. Chem.*, **2012**, *4*, 934-940.
- [2] Licht, S.; Cui, B.; Wang, B.; Li, F.; Lau, J.; Liu, S. *Science*, **2014**, *345*, 637-640.
- [3] Honkala, K.; Hellman, A.; Remediakis, I. N.; Logadottir, A.; Carlsson, A.; Dahl, S.; Christensen, C. H.; Nørskov, J. K. *Science*, **2005**, *307*, 555-558.
- [4] Erisman, J. W.; Sutton, M. A.; Galloway, J.; Klimont, Z.; Winiwarter, W. *Nat. Geosci.*, **2008**, *1*, 636-639.
- [5] Kandemir, T.; Schuster, M. E.; Senyshyn, A.; Behrens, M.; Schlögl, R. *Angew. Chem. Int. Ed.*, **2013**, *52*, 12723-12726.

- [6] Spaulding, D. K.; Weck, G.; Loubeyre, P.; Datchi, F.; Dumas, P.; Hanfland, M. *Nat. Commun.*, **2014**, *5*, 5739.
- [7] Li, J.; Li, H.; Zhan, G.; Zhang, L. *Acc. Chem. Res.*, **2017**, *50*, 112-121.
- [8] Askevold, B.; Nieto, J. T.; Tussupbayev, S.; Diefenbach, M.; Herdtweck, E.; Holthausen, M. C.; Schneider, S. *Nat. Chem.*, **2011**, *3*, 532-537.
- [9] Schrauzer, G. N.; Guth, T. D. *J. Am. Chem. Soc.*, **1977**, *99*, 7189-7193.
- [10] Wu, Q.; Krol, R. *J. Am. Chem. Soc.*, **2012**, *134*, 9369-9375.
- [11] Wang, S.; Hai, X.; Ding, X.; Chang, K.; Xiang, Y.; Meng, X.; Yang, Z.; Chen, H.; Ye, J. *Adv. Mater.*, **2017**, *29*, 1701774.
- [12] Kozuch, S.; Shaik, S. *Acc. Chem. Res.*, **2011**, *44*, 101-110.
- [13] Kitano, M.; Kanbara, S.; Inoue, Y.; Kuganathan, N.; Sushko, P. V.; Yokoyama, T.; Hara, M.; Hosono, H. *Nat. Commun.*, **2015**, *6*, 6731.
- [14] Mortensen, J. J.; Hansen, L. B.; Hammer, B.; Nørskov, J. K. *J. Catal.*, **1999**, *182*, 479-488.
- [15] Jonathan, R.; Jonas, P. *J. Am. Chem. Soc.*, **2016**, *138*, 4243-4248.
- [16] Logadóttir, Á.; Nørskov, J. K. *J. Catal.*, **2003**, *220*, 273-279.
- [17] Siporin, S. E.; Davis, R. J. *J. Catal.*, **2004**, *225*, 359-368.
- [18] He, L.; Jing, L.; Luan, Y.; Wang, L.; Fu, H. *ACS Catal.*, **2014**, *4*, 990-998.
- [19] Rao, N. N.; Dube, S.; Natarajan, M. P. *Appl. Catal. B: Environ.*, **1994**, *5*, 33-42.
- [20] Boucher, D. L.; Davies, J. A.; Edwards, J. G.; Mennad, A. *J. Photoch. Photobio. A: Chem.*, **1995**, *88*, 53-64.
- [21] Dien, N. D.; Phuoc, L. H.; Hien, V. X.; Vuong, D. D.; Chien, N. D. *J. Electron. Mater.*, **2017**, *46*, 3309-3316.
- [22] Pan, X.; Bao, X. *Accounts Chem. Res.*, **2011**, *44*, 553-562.
- [23] Chen, W.; Fan, Z.; Pan, X.; Bao, X. *J. Am. Chem. Soc.*, **2008**, *130*, 9414-9419.
- [24] Chen, G.; Xu, C.; Huang, X.; Ye, J.; Gu, L.; Li, G.; Tang, Z.; Wu, B.; Yang, H.; Zhao, Z.; Zhou, Z.; Fu, G.; Zheng, N. *Nat. Mater.*, **2016**, *15*, 564-569.
- [25] Kibsgaard, J.; Chen, Z.; Reinecke, B. N.; Jaramillo, T. F. *Nat. Mater.*, **2012**, *11*, 963-969.
- [26] Wang, Z.; Liu, B.; Lin, J. *Appl. Catal. A: Gen.*, **2013**, *458*, 130-136.

- [27] Li, L.; Wang, Y.; Vanka, S.; Mu, X.; Mi, Z.; Li, C. *Angew. Chem. Int. Ed.*, **2017**, *56*, 8701-8705.
- [28] Ma, Z.; Xiong, X.; Song, C.; Hu, B.; Zhang, W. *RSC Adv.*, **2016**, *6*, 51106-51110.
- [29] Nakatsuka, K.; Kuwahara, Y.; Mori, K.; Yamashita, H. *Chem. Lett.*, **2015**, *44*, 1691-1693.
- [30] Takagaki, A.; Sugisawa, M.; Lu, D.; Kondo, J. N.; Hara, M.; Domen, K.; Hayashi, S. *J. Am. Chem. Soc.*, **2003**, *125*, 5479-5485.
- [31] Yu, X.; Prevot, M. S.; Guijarro, N.; Sivula, K. *Nat. Commun.*, **2015**, *6*, 8596.
- [32] Hai, X.; Chang, K.; Pang, H.; Li, M.; Li, P.; Liu, H.; Shi, L.; Ye, J. *J. Am. Chem. Soc.*, **2016**, *138*, 14962-14969.
- [33] Wang, X.; Maeda, K.; Thomas, A.; Takanabe, K.; Xin, G.; Carlsson, J. M.; Domen, K.; Antonietti, M. *Nat. Mater.*, **2009**, *8*, 76-80.
- [34] Yang, S.; Gong, Y.; Zhang, J.; Zhan, L.; Ma, L.; Fang, Z.; Vajtai, R.; Wang, X.; Ajayan, P. M. *Adv. Mater.*, **2013**, *25*, 2452-2456.
- [35] Hou, Y.; Laursen, A. B.; Zhang, J.; Zhang, G.; Zhu, Y.; Wang, X.; Dahl, S.; Chorkendorff, I. *Angew. Chem. Int. Ed.*, **2013**, *52*, 3621-3625.
- [36] Dong, G.; Hob, W.; Wang, C. *J. Mater. Chem. A*, **2015**, *3*, 23435-23441.
- [37] Niu, P.; Liu, G.; Cheng, H. *J. Phys. Chem. C*, **2012**, *116*, 11013-11018.
- [38] Xu, C.; Li, K.; Zhang, W. *J. Colloid Interface Sci.*, **2017**, *495*, 27-36.
- [39] Shiraishi, Y.; Shiota, S.; Kofuji, Y.; Hashimoto, M.; Chishiro, K.; Hirakawa, H.; Tanaka, S.; Ichikawa, S.; Hirai, Takayuki. *ACS Appl. Energy Mater.*, **2018**, *1*, 4169-4177.
- [40] Thomas, A.; Fischer, A.; Goettmann, F.; Antonietti, M.; Müller, J.; Schlögl, R.; Carlsson, J. M. *J. Mater. Chem.*, **2008**, *18*, 4893-4908.
- [41] Zhang, X.; Xie, X.; Wang, H.; Zhang, J.; Pan, B.; Xie, Y. *J. Am. Chem. Soc.*, **2013**, *135*, 18-21.
- [42] Kresse, G.; Furthmüller, J. *J. Comput. Mat. Sci.*, **1996**, *6*, 15-50.
- [43] Kresse, G.; Furthmüller, J. *Phys. Rev. B*, **1996**, *54*, 11169-11186.
- [44] Perdew, J. P.; Burke, K.; Ernzerhof, M. *Phys. Rev. Lett.*, **1996**, *77*, 3865-3868.
- [45] Grimme, S.; Antony, J.; Ehrlich, S.; Krieg, S. *J. Chem. Phys.*, **2010**, *132*, 154104.
- [46] Henkelman, G. U.; Uberuaga, B. P.; Jonsson, H. *J. Chem. Phys.*, **2000**, *113*, 9901.

- [47] Zuluaga, S.; Liu, L. H.; Shafiq, N.; Rupich, S. M.; Veyan, J. F.; Chabal, Y. J.; Thonhauser, T. *Phys. Chem. Chem. Phys.*, **2015**, *17*, 957-962.
- [48] Ma, X.; Lv, Y.; Xu, J.; Liu, Y.; Zhang, R.; Zhu, Y. *J. Phys. Chem. C*, **2012**, *116*, 23485-23493.
- [49] Torres, A. E.; Pandiyan, T.; Colmenares, F. *J. Mex. Chem. Soc.*, **2012**, *56*, 287-293.
- [50] Park, S.; An, J.; Potts, J. R.; Velamakanni, A.; Murali, S.; Ruoff, R. S. *Carbon*, **2011**, *49*, 3019-3023.
- [51] Kalytta-Mewes, A.; Spirkl, S.; Tränkle, S.; Hambach, M.; Volkmer, D. *J. Mater. Chem. A*, **2015**, *3*, 20919-20926.
- [52] Norbert, A. L.; and James; G. S. Lange's Handbook of Chemistry, McGraw-Hill, New York, **2005**, *1*.
- [53] Medford, A. J.; Wellendorff, J.; Vojvodic, A.; Studt, F.; Abild - Pedersen, F.; Jacobsen, K. W.; Bligaard, T.; Nørskov, J. K. *Science* **2014**, *345*, 197-200.
- [54] Lee, J.; Pyo, D.; Lee, Y.; Yang, X.; Ryu, S. *Indian J. Eng. Mater. Sci.*, **2010**, *17*, 327-330.
- [55] Kurzydłowski, D.; Derzsi, M.; Budzianowski, A.; Jaglicic, Z.; Kozminski, W.; Mazej, Z.; Grochala, W. *Eur. J. Inorg. Chem.* **2010**, *19*, 2919-2925.
- [56] Jiang, W.; Li, Y.; Han, W.; Zhou, Y.; Tang, H.; Liu, H. *J. Energy Chem.*, **2014**, *23*, 443-452.
- [57] Aika, K. *Catal. Today*, **2017**, *286*, 14-20.
- [58] Saadatjou, N.; Jafari, A.; Sahebdehfar, S. *Chem. Eng. Commun.*, **2015**, *202*, 420-448.
- [59] Peng, X.; Copple, A.; Wei, Q. *J. Appl. Phys.*, **2014**, *116*, 144301.
- [60] Nakada, K.; Fujita, M. *Phys. Rev. B*, **1996**, *54*, 17954-17961.
- [61] Tang, Q.; Cui, Y.; Li, Y.; Zhou, Z.; Chen, Z. *J. Phys. Chem. C*, **2011**, *115*, 1724-1731.
- [62] Bhattacharyya, S.; Kawazoe, Y.; Singhal, A. K. *J. Nanosci Nanotechnol.*, **2012**, *12*, 1899-902.
- [63] Yang, J.; Wang, D.; Han, H.; Li, C. *Acc. Chem. Res.*, **2013**, *46*, 1900-1909.
- [64] Di, Y.; Wang, X.; Thomas, A.; Antonietti, M. *ChemCatChem*, **2010**, *2*, 834-838.
- [65] Jiang, D. E.; Du, M. H.; Dai, S. *J. Chem. Phys.*, **2009**, *130*, 074705.
- [66] Wood, D. W. *Phys. Rev. Lett.*, **1981**, *46*, 749.
- [67] Dean, D. R.; Bolin, J. T.; Zheng, L. *J. Bacteriol.*, **1993**, *175*, 6737-6744.
- [68] Li, H.; Mao, C.; Shang, H.; Yang, Z.; Ai, Z.; Zhang, L. *Nanoscale*, **2018**, *10*, 15429.

[69]Garden, A. L.; Skúlason, E. *J. Phys. Chem. C*, **2015**, *119*, 26554-26559.

TOC

